In silico study of reaction mechanisms and design principles for water oxidation catalysts

Vallés Pardo, J.L.

This chapter is based on:

J.L. Vallés-Pardo, M.C. Guijt, M. Iannuzzi, K.S. Joya, H.J.M. de Groot, F. Buda, ChemPhysChem, 13 (2012) 140-146.

Chapter 4:

Ab-initio molecular dynamics study of water oxidation reaction pathways in mono-Ru catalysts

4.1 Introduction

One of the most important processes in natural and artificial photosynthesis is water oxidation in which water is split into O_2 and H_2 [1]. Inspired by the natural Mn based oxygen evolving complex in photosystem II, a large effort in the last decades has been devoted to synthesize transition metal complexes that can perform the same reaction. A microscopic mechanistic understanding of the natural process is clearly relevant to support the design of artificial devices for fuel generation from solar energy [2, 3]. The most successful artificial catalysts are based on Ru [4, 5], Co [2-4], and more recently Ir complexes [2]. In particular, mono-nuclear molecular catalysts based on Ir(III) have shown to be highly active and robust [10-12]. Density functional theory (DFT) calculations have been also performed to clarify the underlying reaction mechanism in some of these catalysts [10, 11, 13-15]. Available computational chemistry tools have reached a predictive power which is good enough to allow not only the understanding of reaction mechanisms in existing catalysts, but even to assist the design of new catalysts.

In this chapter the first steps in this direction are taken by performing *ab-initio* molecular dynamics (AIMD) simulations with a biasing potential [3] to study mono-Ru catalysts of the type $[(Ar)Ru(X)(bpy)]^+$. Indeed members of this class of novel mono-Ru

catalysts and closely related Ru complexes have been recently synthesized and show water oxidation activity with very high turnover numbers [4, 5]. A catalytic cycle was postulated for the Ir catalyst in Ref. [6] where the X^- ligand is initially replaced by a water molecule. This intermediate then undergoes the first two oxidation steps in which two protons and two electrons are released, yielding a formally Ru^{IV}oxo complex, which is generally assumed to be the active species in the formation of the O-O bond with another water molecule.

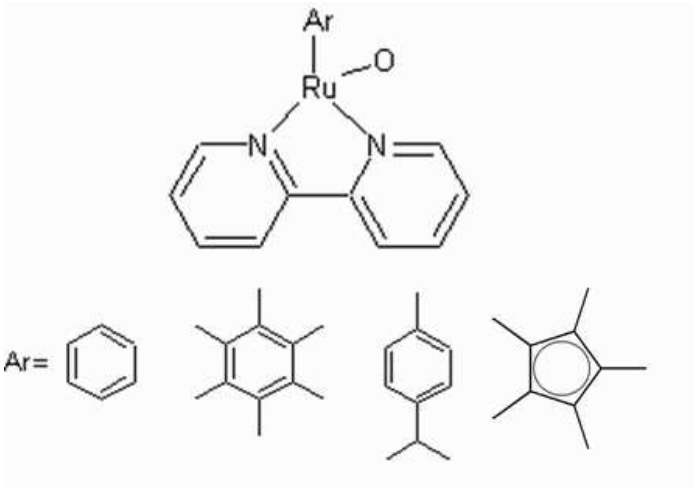

Scheme 4.1. Schematic drawing of the mononuclear Ru catalyst. The aromatic ligands (Ar) are, from left to right, benzene, hexamethylbenzene, cymene, and pentamethylcyclopentadienyl (Cp*)

The Ru complex and the different aromatic ligands (Ar)

considered in this chapter are shown schematically in scheme **4.1**. Here the focus is placed on this crucial reaction step starting from the Ru(IV)oxo intermediate. Possible reaction paths leading to the formation of a hydroperoxo intermediate are analyzed. Most of previous DFT based investigations on similar homogeneous catalysts are performed in the gas phase or with solvation effects included using continuum solvation models. Recent studies have underlined the importance of adding explicit water molecules since they can have a direct role in the reaction mechanism [7, 8]. In this study dynamic effects and an explicit solvent environment are included in order to provide a description of the process that is more realistic than for simulations in vacuum.

4.2 Computational details

The *ab-initio* molecular dynamics (AIMD) simulations [7] in this work are performed with the CP2K program [8]. The OPBE exchange-correlation functional for the DFT electronic structure calculations is used [9]. The choice of this non-hybrid functional is mainly dictated by the computational efficiency in the AIMD and is justified by previous work where it has been shown to give an accurate description of several transition metal complexes [15-18]. Additional tests were performed to

validate the OPBE results using the non-hybrid functional BLYP [10, 11] and the hybrid functionals B3LYP and B3LYP*, with different amounts of exact exchange, 0.2 and 0.15, respectively [11, 12]. The ADF program was used for the calculations with the hybrid functionals [13, 14]. The CP2K program employs a mixed basis set approach with Gaussian type orbitals (GTO) and plane waves (PWs) [15]. GTO functions are used to expand the molecular orbitals and the charge density in real space, whereas PWs are used for the representation of the charge density in reciprocal space. An energy cut-off of 280 Ry is used for the plane-waves basis set. The TZVP-MOLOPT-GTH [16] Gaussian basis set is chosen for all the atoms in the catalyst except ruthenium for which a DZVP-MOLOPT-GTH is used. The water molecules close to the catalyst and involved in the reaction are treated at the TZVP-MOLOPT-GTH level, whereas the DZVP-MOLOPT-GTH is used for all the other water molecules. Pseudopotentials of the GTH form for all the elements [15, 17, 18] are used. The pseudopotential for Ru is generated with 16 valence electrons. In the ADF calculations a TZP Slater type basis set is applied.

Due to the presence of π-cation interactions between the metallic centre and the aromatic ligand, it is crucial to include van der Waals corrections. In all the AIMD simulations the DFT-D2 van der Waals correction by Grimme is applied [19, 20]. Since the OPBE functional does not have its own set of correction parameters, the Grimme parameters for PBE are used instead. Periodic boundary conditions

(PBC) are applied in the simulations with explicit solvent, while for the gas phase simulations without PBC the Martina-Tuckerman approach is used for the Poisson solver [21]. For the AIMD simulations a time step Δt = 0.5 fs is considered. In order to explore possible reaction pathways, a very useful tool is the metadynamics approach proposed by Laio and Parrinello [3], which is efficiently implemented in the CP2K code. The metadynamics is a coarse-grained dynamics on the free-energy surface (FES) defined by a few collective variables (*e.g.*, the distance between two atoms) using an adaptive bias potential in order to escape from a local minimum. At each metadynamics step the evolution of the collective variables is guided by a generalized force that combines the action of the thermodynamic force, which would trap the system in a free energy minimum, and a history-dependent force that disfavours configurations already visited. This history-dependent potential is built as a sum of Gaussian functions centered in the explored values of the collective variables [3]. The height and the width of the Gaussian are 10^{-3} Hartree and 0.02 a.u., respectively. In the simulations the collective variables are evolved with one metadynamics step every 20 AIMD time steps. In this way a quick exploration of the reaction pathway can be done, at the expense of accuracy in probing the free-energy surface along the collective variable. For a preliminary estimate of the free-energy, a thermodynamic integration technique with constrained MD [22, 23] can be used instead. Six points along the Ox-Ow distance are considered in the range 1.45-2.25 Å and for each

point an equilibration of the system for about 1.5 ps is performed. This combination of the metadynamics approach and constrained MD is found to be computationally most efficient.

Simulations with explicit solvent environment are performed in an orthorhombic box of 16x15.5x15 $Å^3$ containing the Ru catalyst and 73 water molecules, which are all treated at the quantum-mechanical level. Before starting the AIMD simulations, the solvent is equilibrated with force field MD simulations while keeping the transition metal complex fixed. First the volume of the box is adjusted with a constant pressure simulation and then the system is further equilibrated at constant volume and constant room temperature. For these preliminary steps the Discovery Studio software [24] is used with the CHARMM force field and the TIP3P model [25].

4.3 Results and discussion

4.3.1 Characterization of the [(Ar)Ru(O)(bpy)]$^{+2}$ intermediate

The Ru(IV)oxo complex that is assumed to be the active species in the O-O bond formation is the starting point of the investigation. The initial geometry has been generated starting from the DFT optimized coordinates of the analogous Ir based catalysts provided in Ref. [6] and

by substituting the Ir atom with Ru. The geometry of the $[(Ar)Ru(O)(bpy)]^{2+}$ species is optimized with different aromatic ligands and for different spin states using various functionals. The inclusion of van der Waals corrections is crucial for the structural stability of the complex, as without these corrections the Ru-Ar bond breaks during the geometry optimization. Table **4.1** shows the comparison of the relative energies for different possible multiplicities. All the functionals, both hybrid and non-hybrid, give consistently the same lowest energy spin state. In particular, the triplet is the ground-state for the benzene and hexamethylbenzene ligands, while the doublet is the ground-state for the complex with the Cp* ligand. Quantitative differences between the hybrid and non-hybrid functionals, with the latter usually giving a smaller energy splitting between the two lowest states compared to the hybrid functionals, are present. Given that all functionals considered here provide consistent results, the OPBE functional was used for the subsequent AIMD simulations, because of its superior computational efficiency (see also the computational details section).

In Table **4.2** a few relevant geometrical parameters and effective RESP atomic charges [26] obtained for the most stable multiplicity using the OPBE functional are shown. These results show the effect of using different aromatic ligands on the geometric and electronic structure of the catalyst. It appears that the choice of the aromatic ring has only moderate effect on the distance between the ruthenium and the oxo ligand (Ru-O). Also the average value of the two distances between

the ruthenium and the nitrogen atoms of the bipyridine (Ru-N) are reported. The distance between ruthenium and the centre of the aromatic ring (Ru-Ar) is also an interesting parameter since a weak interaction between them could be a source of instability in the catalyst. This distance becomes shorter for increasing ring size. The effective RESP charges for ruthenium, oxygen and the aromatic ring are quite sensitive to the choice of the ligand. Specifically, the oxo ligand carries a negative charge, which increases for aromatic rings richer in electrons.

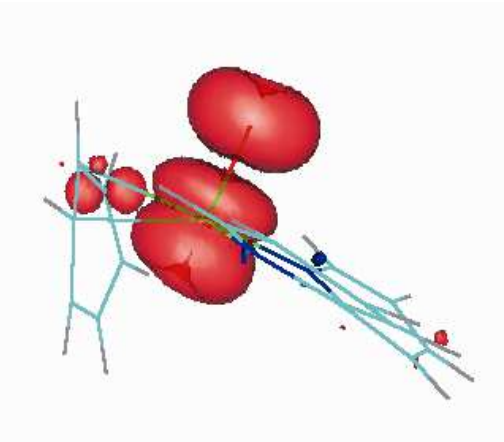

Figure 4.1. Spin density isosurface for the [(benzene)Ru(O)(bpy)]$^{2+}$ in the triplet state. This figure has been produced with gOpenMol.

In Figure **4.1** the spin density for the [(benzene)Ru(O)(bpy)]$^{2+}$ complex in the triplet state is shown, clearly pointing to a strong radical character of the oxo ligand, which will be indicated in the following as

the oxyl radical. This radical character has been considered a key feature to activate the O-O bond formation [27].

Table 4.1. Comparison of the energies of the $[(Ar)Ru(O)(bpy)]^{2+}$ for different multiplicities and calculated using various functionals. The values are given in kcal mol^{-1} and are relative to the lowest energy spin state.

Benzene

	BLYP	OPBE	B3LYP	B3LYP*
Triplet	0	0	0	0
Singlet	3.5	6.5	13.9	13.2
Quintet	24.3	89.7	47.0	48.0

Hexamethylbenzene

	BLYP	OPBE	B3LYP	B3LYP*
Triplet	0	0	0	0
Quintet	16.4	44.0	9.7	10.4
Singlet	224.0	7.6	20.3	19.7

Cp*

	BLYP	OPBE	B3LYP	B3LYP*
Doublet	0	0	0	0
Quartet	22.9	22.6	29.7	29.5
Sextet	84.0	87.2	106.1	102.0

Table 4.2. Geometrical parameters and effective RESP atomic charges for the [(Ar)Ru(O)(bpy)]$^{2+}$ complex using different aromatic rings. These results are obtained with the OPBE functional for the lowest energy spin state. Distances are given in Å, angles in degrees.

Geometrical parameters

	Ru-O	Ru-Ar	Ru-N	O-Ru-Ar
Benzene	1.74	1.90	2.11	125.88
Hexamethylbenzene	1.73	1.80	2.25	123.87
Cp*	1.71	1.86	2.03	136.04

Effective RESP charges

	Ru	O	Ar
Benzene	1.86	-0.45	0.30
Hexamethylbenzene	3.62	-1.10	0.57
Cp*	3.45	-1.22	0.19

4.3.2 AIMD simulations for the O-O bond formation

In this section two different reaction mechanisms for the O-O bond formation are under investigation using metadynamics simulations, as described in the computational details section. In the first scenario it is assumed that the incoming water molecule first coordinates to the Ru, thus creating a heptacoordinated intermediate, assuming that these aromatic rings are treated as tridentate ligands. This is followed by a second step in which the O-O bond could be formed. In the second case

it is considered that the incoming water molecule attacks the oxyl radical for a direct O-O reaction. These two suggested pathways are similar to those addressed in a recent theoretical study on ruthenium water oxidation catalysts [28].

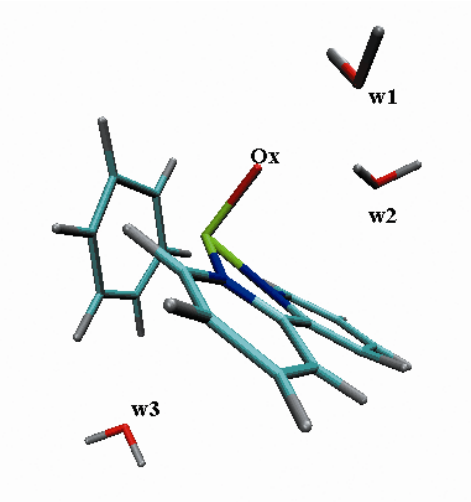

Figure 4.2. Optimized geometry of the [(benzene)Ru(O)(bpy)]$^{2+}$ intermediate including three water molecules. This image was made with VMD [29]

In order to assess the importance of the inclusion of an extensive solvation at the quantum-mechanical level metadynamics simulations for the [(benzene)Ru(O)(bpy)]$^{2+}$ catalyst are performed, both in vacuum and in an explicit solvent environment. For the simulations in vacuum the optimized Ru complex plus three water molecules in its proximity is taken as starting geometry (see Figure **4.2**). For the simulations in the

presence of an explicit solvent environment the catalyst plus 73 water molecules are included in the molecular dynamics box with periodic boundary conditions (see also the computational details section).

4.3.2.1 Ru-Ow3 approach

In the first AIMD simulation for this approach the $[(Benzene)Ru(O)(bpy)]^{2+}$ complex plus three water molecules are included: w1, w2 close to the oxyl radical and w3 at 3.5 Å from the Ruthenium atom on the opposite side (see Figure **4.2**). The collective variable (CV) used in this simulation is the Ru-Ow3 distance with a maximum allowed value of 3.7 Å. In Figure **4.3** the Ru-Ow3 and the Ru-benzene distances along the AIMD trajectory are shown. The benzene breaks its coordination bond when the incoming water enters the coordination shell of the metal (Ru-Ow3≈2.7 Å), suggesting that this pathway is unfeasible. It should be pointed out that the biasing potential builds up also when the water is coordinated to the Ru (see Figure **4.3**, after about 1 ps). This is why the water eventually leaves the Ru coordination shell in the second part of the trajectory.

In order to check if the observed structural instability of the catalyst is related to the specific choice of the aromatic ligand, or to the missing water environment, additional simulations using the same setup were performed: First the benzene ligand was substituted with hexamethylbenzene and cymene and then the same reaction path was analysed in vacuum. In addition the benzene was reconsidered in a

water solvated environment. In all these simulations a similar behaviour with the aromatic ligand leaving the coordination shell of the metal is present. In Figure **4.3** the results obtained in vacuum and in solvated environment for the benzene case are shown. The simulations reveal how the degradation of the catalyst is very similar in both cases, with the water environment only slightly slowing down the process. It can be concluded that the heptacoordinated form of the Ruthenium is not stable for this class of catalysts.

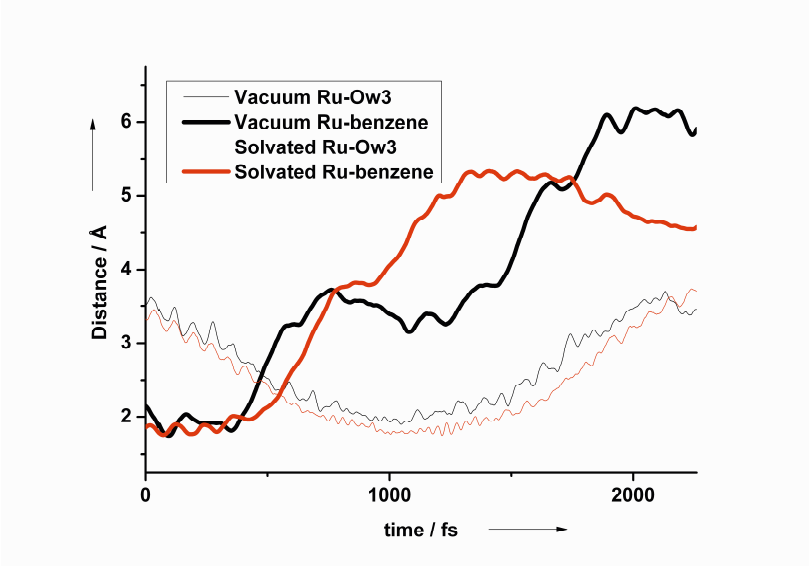

Figure 4.3. Relevant geometrical parameters along the metadynamics simulation of the [(benzene)Ru(O)(bpy)]$^{2+}$ complex, in which the Ru-Ow3 distance is the collective variable. For the atomic labeling in the legend we refer to Figure 4.2.

4.3.2.2 Ox-Ow1 approach

The starting geometry for these metadynamics simulations is the same as used in the previous case (Figure **4.2**), but here the CV is the distance between the oxyl radical and the oxygen of water w1 (Ox-Ow1) with an initial value of 3.5 Å and a maximum allowed value of 3.7 Å. When the Ox-Ow1 distance becomes less than ~1.8 Å, an increase of the Ru-Ox and of the Ow1-Hw1 distances occurs.

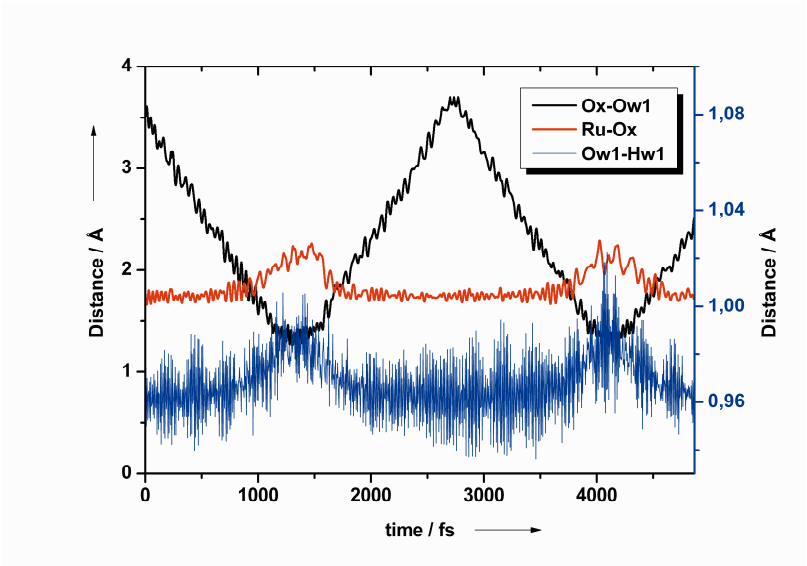

Figure 4.4. Relevant geometrical parameters along the metadynamics simulation of the [(benzene)Ru(O)(bpy)]$^{2+}$ in the gas phase, with the Ox-Ow1 distance as the collective variable. The atomic labelling in the legend refers to Figure 4.2. The right axis refers to the Ow1-Hw1 distance (blue line).

This observation is well in line with expectations. When the bond between Ox and Ow has been established, the interaction between Ruthenium and the oxyl radical becomes weaker since the double bond character is lost. On the other hand it is also expected that the O-O bond formation would be accompanied by a proton jump from the reactant water, thus this slight increase of the Ow1-Hw1 distance can be interpreted as the initiation of a proton jump. It is clear that a proper proton acceptor in this simulation is still missing.

In order to address the question about the importance of the solvent environment for this reaction, the same metadynamics simulation in the presence of explicit water molecules surrounding the catalyst is performed (see Computational Details section). The results are illustrated in Figure **4.5**, where the relevant geometrical parameters describing the reaction are plotted. It should be emphasized again that only the distance between the oxygen of the water molecule (Ow1) and the oxyl radical (Ox-Ow1, black line) is driven by the adaptive biasing potential, while all other structural changes occur spontaneously. When Ox-Ow1 is about 1.8 Å an increase in the Ru-Ox distance (red line) and an increase in the water bond length Hw1-Ow1 (blue line) can be observed, matching the result of the previously described simulation in vacuum. However, a decrease in the distance between Hw1 and the oxygen of a second water molecule (Ow2, green line) is also occurring. Soon after the Ox-Ow1 distance has reached a value of ~1.4 Å, indicating the formation of the O-O bond, one proton of the reactant

water jumps on the second water, thus forming a hydronium ion OH_3^+. In Figure **4.6**, a snapshot of the simulation after 1.7 ps, clearly shows the formation of the Ru-OOH intermediate and of a hydronium ion. Figure **4.5** also shows that if the metadynamics simulation continues, the biasing potential will fill the local minimum in the free energy landscape corresponding to this intermediate state and the reaction is reversed.

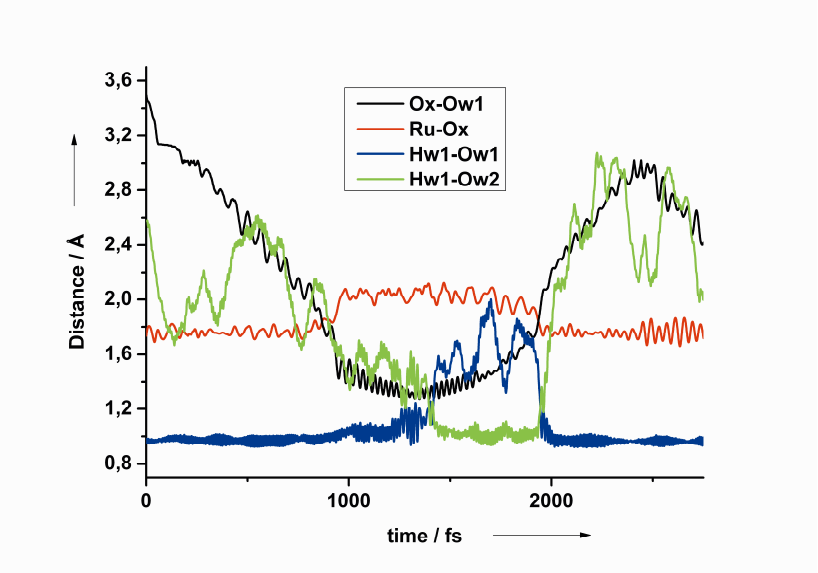

Figure 4.5. Relevant geometrical parameters along the metadynamics simulation of the solvated [(Benzene)Ru(O)(bpy)]$^{2+}$ complex, in which the Ox-Ow1 distance is the collective variable. The atomic labelling in the legend refers to Figure 4.2

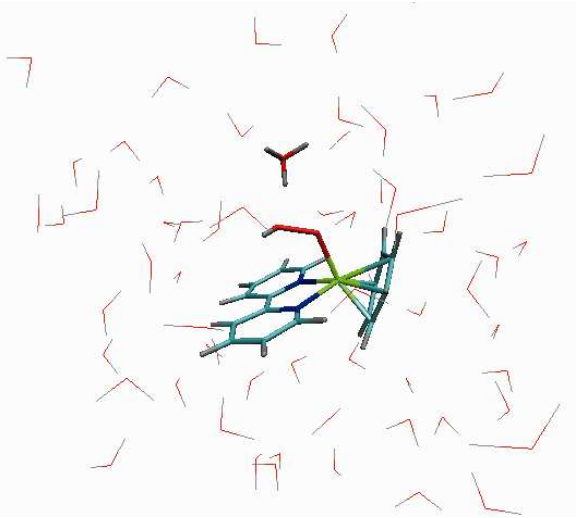

Figure 4.6. Hydroperoxo intermediate in solvated environment. The hydronium ion formed in the simulation is also highlighted. This snapshot is taken after 1.7 ps of simulation. The image was made with VMD [29]

For an estimate of the free-energy profile a thermodynamic integration technique with constrained MD is used, in which each initial configuration is extracted from the metadynamics trajectory. The preliminary estimated free-energy shows a low activation barrier of around 10 kcal mol^{-1} and a $\Delta G \approx -10$ kcal mol^{-1} between the Ru-OOH intermediate and the initial complex, indicating that this reaction step is exothermic. The transition state is found for an Ox-Ow1 distance between 1.85 and 1.95 Å. These constrained AIMD simulations show that the proton jumps spontaneously to the water environment when the

Ox-Ow1 distance is shorter than the transition state value. Moreover, the oxo ligand apparently never acts as a proton acceptor in the simulations, in contrast with the suggestion presented in Ref. [6]. Two additional AIMD simulations of a few ps at room temperature are also performed, without any constraints, for the solvated initial Ru-oxyl and the final Ru-hydroperoxo intermediates to verify that indeed these two intermediates are stable in water.

4.3.3 Characterization of the [(benzene)Ru(OOH)(bpy)]$^{+1}$ intermediate and the transition state

In this section the structural and electronic properties of the Ru-OOH intermediate and the transition state found in the AIMD simulations are analyzed. In Table **4.3** a comparison between geometrical parameters and relative energies obtained in the gas phase is presented. For a proper energetic comparison, the same cubic simulation box size, with a side length of 18 Å, is considered for each supramolecular complex. Both the initial complex (Ru-oxyl) and the transition state (TS) include two water molecules, while for the hydroperoxo intermediate the hydronium cation is included. In this way each calculation has the same number of atoms and total charge.

There are a few important considerations emerging from this analysis. First, during the oxygen bond formation (Ox-Ow1) the Ru-Ox

distance increases as expected, while the Ru-benzene distance decreases. During the geometry optimization of the Ru-OOH complex with the hydronium cation, one proton is transferred from the hydronium to the Ox forming a hydrogen peroxide ligand (Ru-HOOH). This final complex resembles closely the species found for the similar Ir catalyst studied in Ref. [6]. This result is at variance with the behavior observed in the AIMD simulations in water, where the hydronium is stabilized by the solvation shell, underlining the importance of the solvent environment.

Table 4.3. Comparison between the energy in vacuum of the initial complex (Ru-oxyl) including two water molecules, the transition state (TS) and final intermediate including the hydronium (Ru-HOOH). Geometrical parameters for the hydroperoxo complex (Ru-OOH) are also reported. Distances are in Å and energies in kcal mol^{-1}. The atomic labelling refers to Figure 4.2. The lowest energy multiplicity is indicated.

	Ru-Ox	Ru-Benzene	Ox-Ow1	Relative energy	Multiplicity
Ru-oxyl	1.75	1.77	3.08	0	Triplet
TS	1.80	1.72	1.93	24.3	Singlet
Ru-HOOH	2.20	1.63	1.43	11.0	Singlet
Ru-OOH	2.00	1.63	1.43	-	Singlet

A preliminary characterization of the transition state in vacuum including the reactant water and the water accepting the proton is shown in Figure **4.7** and some of the corresponding geometrical

parameters are given in Table **4.3**. In particular a d(Ox–Ow1)=1.93 Å is found and the second water (w2) is ready to accept the proton with d(Ow2–Hw1)=1.57 Å. The TS energy is about 24 kcal mol^{-1} higher than for the reactant, which compares well with the value of 24.0 kcal mol^{-1} found by Blakemore *et al.* for the analogous Ir catalyst when they include two water molecules [6]. However, the transition state found for the Ir complex has a distance d(Ox–Ow1)=1.50 Å, which is much shorter than for our system and very close to the equilibrium O-O distance in the hydroperoxo intermediate. In fact another transition state with a similar Ox–Ow1 short distance is found, which according to the vibrational analysis corresponds to the proton transfer step from the reactant water to the second water and is not representative of the actual transition state for the O-O bond formation. From the comparison with the free-energy barrier estimated in the water environment, it could be concluded that the solvent is important in facilitating this reaction step. The energy difference between the initial and the final complex in vacuum cannot be directly compared with the result in water since two different intermediates are obtained. Therefore the results obtained with an explicit solvent are not only quantitatively but also qualitatively different from those obtained in the gas phase.

An important point that is extensively discussed in the literature for this class of catalysts is the oxidation state of the metallic centres. To check if the Ru atom increases or decreases its oxidation state during this reaction step, a RESP charge analysis of the optimized

initial (Ru-oxyl) and final (Ru-OOH) intermediate states in the gas phase is performed. This analysis clearly shows that the ruthenium increases its positive charge in spite of the decrease of the overall charge of the hydroperoxo intermediate to +1. The excess positive charge on the Ru is overcompensated by an increase in the negative charge, predominantly on the benzene and in the bipyridine ligands. This increased charge polarization in the complex can explain the shortening of the Ru-benzene distance due to a stronger electrostatic interaction.

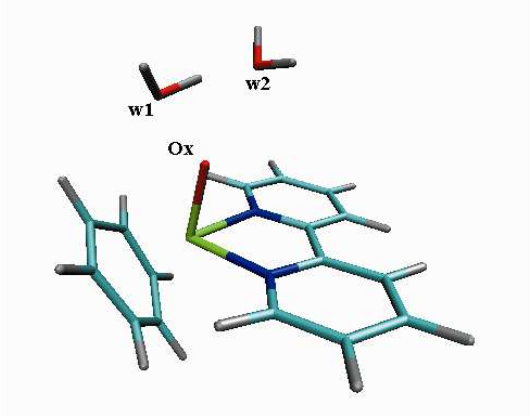

Figure 4.7. Transition state of the Ru catalyst with a benzene ligand and including two water molecules. This image was made with VMD [29]

Finally, in Table **4.3** the most stable spin multiplicity for the hydroperoxo intermediate is listed, which turns out to be a singlet,

unlike the initial complex where a triplet state was found. Therefore, the results point to the occurrence of a spin-crossover during the reaction. This spin-crossover appears to be located at (or close to) the transition state, where the singlet and triplet states differ in energy by only ~1 kcal mol^{-1}. This result is reminiscent of the two-state reactivity discussed by Shaik and co-workers for Fe complexes [30].

4.4 Conclusions

This chapter shows how the *ab-initio* molecular dynamics approach with an adaptive bias potential can be an important tool to efficiently explore potential reaction paths for water oxidation reactions at room temperature and with an explicit inclusion of the water environment. The focus of the analysis is a class of mononuclear ruthenium catalysts that are inspired by recently synthesized analogous iridium-based catalysts. In the computer simulations it is easy to check the effect of modifying the ligands and/or the metal centres and the predictive range of this type of *in silico* studies can assist the development of new, efficient and robust catalysts for artificial photosynthesis.

The reaction path involving first a coordination step of the reactant water to the metal centre appears unlikely since it leads to a structural

instability of the catalyst with the breaking of the metal-aromatic ligand coordination bond. The alternative path, in which the reactant water directly attacks the oxyl radical, leads to the formation of the O-O bond resulting in a Ru-hydroperoxo complex and to the release of one proton into the solvent environment. This simulation shows that the proton release occurs spontaneously at room temperature and thus is not the rate-limiting step. Moreover, it underlines the crucial role played by the solvent in facilitating the formation of the hydroperoxo intermediate with an activation free-energy of only about 10 kcal mol^{-1}. From the analysis of the charge distribution in the complex before and after the reaction, this step in the catalytic cycle can be interpreted as a proton-coupled electron transfer (PCET) process, since electron charge moves from the metallic centre to the aromatic ring. In this scheme the aromatic ligand plays the role of an electronic charge buffer, facilitating the electronic steps in the catalytic cycle. Interestingly, a spin-crossover appears to occur along this reaction path since the final intermediate is found to be a singlet while the initial Ru-oxyl complex is a triplet state. Further investigations are ongoing to get a more accurate estimate of the free energy profile and the effect of different aromatic ligands.

4.5 Bibliography

1. Lubitz, W., Reijerse, E.J., Messinger, J., *Energy & Environmental Science*, 1 (**2008**) 15-31.
2. McDaniel, N.D., Coughlin, F.J., Tinker, L.L., Bernhard, S., *Journal of the American Chemical Society*, 130 (**2007**) 210-217.
3. Laio, A., Parrinello, M., *Proceedings of the National Academy of Sciences of the United States of America*, 99 (**2002**) 12562-12566.
4. Joya, K.S., de Groot, H.J.M., *Metal complex and use as multielectron catalyst*, **2011**, PCT/NL2011/050673
5. Bernet, L., Lalrempuia, R., Ghattas, W., Mueller-Bunz, H., Vigara, L., Llobet, A., Albrecht, M., *Chemical Communications*, 47 (**2011**) 8058-8060.
6. Blakemore, J.D., Schley, N.D., Balcells, D., Hull, J.F., Olack, G.W., Incarvito, C.D., Eisenstein, O., Brudvig, G.W., Crabtree, R.H., *Journal of the American Chemical Society*, 132 (**2010**) 16017-16029.
7. Marx, D., Hutter, J., *Ab Initio Molecular Dynamics: Basic Theory and Advanced Methods*, Cambridge University Press, Cambridge, **2009**.
8. The CP2K developers group. http://cp2k.berlios.de/.
9. Swart, M., Ehlers, A.W., Lammertsma, K., *Molecular Physics*, 102 (**2004**) 2467-2474.
10. Becke, A.D., *Physical Review A*, 38 (**1988**) 3098-3100.
11. Lee, C., Yang, W., Parr, R.G., *Physical Review B*, 37 (**1988**) 785-789.
12. Becke, A.D., *The Journal of Chemical Physics*, 98 (**1993**) 5648-5652.
13. te Velde, G., Bickelhaupt, F.M., Baerends, E.J., Fonseca Guerra, C., van Gisbergen, S.J.A., Snijders, J.G., Ziegler, T.,

Journal of Computational Chemistry, 22 (**2001**) 931-967.
14. ADF2007.2001, SCM, Theoretical Chemistry, Vrije Universiteit, Amsterdam, The Netherlands, <http://www.scm.com/>
15. Krack, M., *Theoretical Chemistry Accounts*, 114 (**2005**) 145-152.
16. VandeVondele, J., Hutter, J., *The Journal of chemical physics*, 127 (**2007**) 114105.
17. Goedecker, S., Teter, M., Hutter, J., *Physical Review B*, 54 (**1996**).
18. Hartwigsen, C., Goedecker, S., Hutter, J., *Physical Review B*, 58 (**1998**).
19. Grimme, S., *Journal of Computational Chemistry*, 27 (**2006**) 1787-1799.
20. Grimme, S., Antony, J., Ehrlich, S., Krieg, H., *The Journal of chemical physics*, 132 (**2010**) 154104.
21. Martyna, G.J., Tuckerman, M.E., *The Journal of Chemical Physics*, 110 (**1999**) 2810-2821.
22. Sprik, M., Ciccotti, G., *The Journal of Chemical Physics*, 109 (**1998**) 7737-7744.
23. den Otter, W.K., Briels, W.J., *The Journal of Chemical Physics*, 109 (**1998**) 4139.
24. Accelrys Software Inc., Discovery Studio Modeling Environment http://accelrys.com/.
25. MacKerell, A.D., Bashford, D., Bellott, Dunbrack, R.L., Evanseck, J.D., Field, M.J., Fischer, S., Gao, J., Guo, H., Ha, S., Joseph-McCarthy, D., Kuchnir, L., Kuczera, K., Lau, F.T.K., Mattos, C., Michnick, S., Ngo, T., Nguyen, D.T., Prodhom, B., Reiher, W.E., Roux, B., Schlenkrich, M., Smith, J.C., Stote, R., Straub, J., Watanabe, M., WiÃ³rkiewicz-Kuczera, J., Yin, D., Karplus, M., *The Journal of Physical Chemistry B*, 102 (**1998**) 3586-3616.
26. Laio, A., Gervasio, F.L., VandeVondele, J., Sulpizi, M., Rothlisberger, U., *The Journal of Physical Chemistry B*, 108 (**2004**) 7963-7968.

27. Lundberg, M., Blomberg, M.R.A., Siegbahn, P.E.M., *Inorganic chemistry*, 43 (**2004**) 264-274.
28. Wang, L.-P., Wu, Q., Van Voorhis, T., *Inorganic Chemistry*, 49 (**2010**) 4543-4553.
29. The molecular representations have been made with the program VMD owned by the Theoretical and Computational Biophysics Group, NIH Resource for Macromolecular Modeling and Bioinformatics, at the Beckman Institute, University of Illinois at Urbana-Champaign: <http://www.ks.uiuc.edu/Research/vmd/>
30. Shaik, S., de Visser, S., Ogliaro, F., Schwarz, H., Schroder, D., *Current Opinion in Chemical Biology*, 6 (**2002**) 556-567.